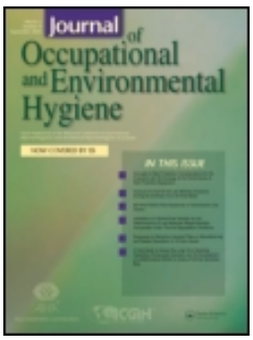

Journal of Occupational and Environmental Hygiene

ISSN: 1545-9624 (Print) 1545-9632 (Online) Journal homepage: http://www.tandfonline.com/loi/uoeh20

# Relationships Among Particle Number, Surface Area, and Respirable Mass Concentrations in Automotive Engine Manufacturing

William A. Heitbrink , Douglas E. Evans , Bon Ki Ku , Andrew D. Maynard , Thomas J. Slavin & Thomas M. Peters

**To cite this article:** William A. Heitbrink , Douglas E. Evans , Bon Ki Ku , Andrew D. Maynard , Thomas J. Slavin & Thomas M. Peters (2008) Relationships Among Particle Number, Surface Area, and Respirable Mass Concentrations in Automotive Engine Manufacturing, Journal of Occupational and Environmental Hygiene, 6:1, 19-31, DOI: 10.1080/15459620802530096

**To link to this article:** https://doi.org/10.1080/15459620802530096

*Journal of Occupational and Environmental Hygiene*, 6: 19–31
ISSN: 1545-9624 print / 1545-9632 online
DOI: 10.1080/15459620802530096

# Relationships Among Particle Number, Surface Area, and Respirable Mass Concentrations in Automotive Engine Manufacturing

**William A. Heitbrink,[1] Douglas E. Evans,[2] Bon Ki Ku,[2] Andrew D. Maynard,[3] Thomas J. Slavin,[4] and Thomas M. Peters[1]**

[1]Department of Occupational and Environmental Health, University of Iowa, Iowa City, Iowa
[2]National Institute for Occupational Safety and Health, Division of Applied Research and Technology, Cincinnati, Ohio
[3]Woodrow Wilson International Center for Scholars, Washington, D.C.
[4]International Truck and Engine Corporation, Warrenville, Illinois

*This study investigated the relationships between particle number, surface area, and respirable mass concentration measured simultaneously in a foundry and an automotive engine machining and assembly center. Aerosol concentrations were measured throughout each plant with a condensation particle counter for number concentration, a diffusion charger for active surface area concentration, and an optical particle counter for respirable mass concentration. At selected locations, particle size distributions were characterized with the optical particle counter and an electrical low pressure impactor. Statistical analyses showed that active surface area concentration was correlated with ultrafine particle number concentration and weakly correlated with respirable mass concentration. Correlation between number and active surface area concentration was stronger during winter ($R^2 = 0.6$ for both plants) than in the summer ($R^2 = 0.38$ and 0.36 for the foundry and engine plant respectively). The stronger correlation in winter was attributed to use of direct-fire gas fired heaters that produced substantial numbers of ultrafine particles with a modal diameter between 0.007 and 0.023 $\mu$m. These correlations support findings obtained through theoretical analysis. Such analysis predicts that active surface area increasingly underestimates geometric surface area with increasing particle size, particularly for particles larger than 100 nm. Thus, a stronger correlation between particle number concentration and active surface area concentration is expected in the presence of high concentrations of ultrafine particles. In general, active surface area concentration may be a concentration metric that is distinct from particle number concentration and respirable mass concentration. For future health effects or toxicological studies involving nano-materials or ultrafine aerosols, this finding needs to be considered, as exposure metrics may influence data interpretation.*

**Keywords** active surface area concentration, comparison between exposure metrics, respirable mass concentration, ultrafine number concentration

Address correspondence to: William A. Heitbrink, Department of Occupational and Environmental Health, University of Iowa, 102 IREH, 100 Oakdale Campus, Iowa City, IA 52242-5000; e-mail: william-heitbrink@uiowa.edu.

The mention of any company or product does not constitute an endorsement by the Centers for Disease Control and Prevention. The findings and conclusions in this report are those of the authors and do not necessarily represent the views of the National Institute for Occupational Safety and Health.

## INTRODUCTION

Ultrafine particles are commonly encountered in automotive foundries and machining centers as unintended byproducts from manufacturing operations.[1] Substantial quantities of submicrometer particles are generated by foundry operations, such as the melting and subsequent pouring of liquid alloy into molds.[2] Although most machining operations produce aerosols larger than 1 $\mu$m,[3–10] many operations produce a submicrometer component if "hot" processes such as welding,[11,12] heat treating, grinding,[13] and high-speed machining[14,15] are involved. For example, the frictional forces involved in grinding may result in surface temperatures in excess of 550°C.[16]

Although most occupational exposure limits for aerosols are based on mass concentration, additional metrics are being considered to assess worker exposure to ultrafine particles.[17,18] Particle number or surface area concentration may better reflect adverse cardiopulmonary outcomes than respirable mass concentration for nonsoluble, ultrafine particles (diameter < 100 nm).[19–22] Moreover, the mass concentration of ultrafine particles is often negligible compared with that of larger particles. Thus, control measures that focus on reducing aerosol

mass concentrations in the workplace may not necessarily translate into improved worker health if ultrafine particle exposures persist.[23]

From a practical standpoint, many questions remain as to how different metrics should be measured in occupational settings. For particle surface area concentration, as an example, the traditional approach is to determine the surface area of bulk material through gas adsorption, commonly known as the BET method.[24] However, the quantities of particulate required to measure surface area by BET (milligrams) require that airborne sample collection is conducted at high flow rates and for long sampling periods, which may not be possible or practical for most workplace monitoring situations. Furthermore, this method does not lend itself to real-time measurements that may aid in identifying sources or "hot spots." Alternatively, estimates of particle surface area concentration may be derived from measurements of particle number concentration by size. However, instruments that provide these data are generally expensive, not particularly portable for routine use, and not well suited for many workplace settings.

Instruments that directly provide a real-time measure of particle surface area concentration, known as diffusion chargers, are attractive because they are compact and portable, economical, battery operated, and field robust. However, diffusion chargers measure the *active* surface area concentration, which may be different in many cases from the *physical* or *geometric* surface area concentration on which toxicological data are based.

Active surface area is defined as the surface of a particle that is involved in the interactions with the surrounding gas.[25] In the free molecular regime, where particle diameter is much smaller than the mean free path of the surrounding gas, active surface area is equivalent to the geometric surface area for spherical particles, and proportional to particle diameter squared. However, as particle size increases, this relationship is lost and active surface area of a particle increases proportionally to particle diameter.[25]

As discussed in the following section, active surface area is the result of phenomena that occur in the gas phase, yet interactions between deposited air contaminants and the human respiratory tract, for example, generally take place in fluids. From a practical perspective, instruments that provide active surface area are suitable for exposure assessments in actual workplaces. Other metrics such as particle number concentration measured by hand-held condensation particle counters (CPCs) or respirable mass concentration measured by traditional gravimetric methodology may be acceptable indicators of exposure to ultrafine particles in certain cases.

A comparison of these different metrics in workplaces is needed to understand the limitations inherent to each technology within the context of protecting worker health from exposure to ultrafine particle and evaluating the relationship between exposure and health effects for ultrafine aerosols. Because of the uncertainty as to the most appropriate exposure metric for ultrafine aerosols and nanomaterials, the simultaneous measurement of particle number, surface area and mass concentrations has been recommended for exposure assessments.[26]

Thus, this study explores the relationships between particle number concentration, active surface area concentration, and respirable mass concentration measured in automotive engine manufacturing environments. Particle concentrations according to these different metrics were measured simultaneously with direct-reading instruments on 942 occasions at a multitude of locations within an engine machining and assembly facility and an adjacent foundry. Theoretical considerations for the measurement of particle surface area concentration are presented, followed by an analysis of the relationships among collocated measurements of particle concentrations by these different metrics.

## Considerations in Measuring Particle Surface Area Concentration

As extensively discussed by Keller et al.,[25] the active surface area of a particle is the area of the particle that interacts with the gas. The product of this active surface area ($A_{active}$) and particle mobility (B) has been observed experimentally to be a constant up to a particle size of 0.75 $\mu$m. This expression is stated mathematically as:[27]

$$B \bullet A_{active} = \text{const.} \quad \textbf{(1)}$$

The mobility of a particle, in the free molecular range, may be expressed as:

$$B = \frac{\lambda}{\pi \delta \eta d_p^2} \quad \textbf{(2)}$$

where $\lambda$ is the mean free path; $\eta$ is the viscosity of air and $\delta$ is a scattering parameter that expresses the tendency of a gas molecule to bounce from the surface of the particle.[27,28]

Based on Friedlander's formula for friction and mobility, $\delta$ may be estimated as a function of $\alpha$:

$$\delta = \frac{2}{3}\left[1 + \frac{\pi}{8}\alpha\right] \quad \textbf{(3)}$$

where $\alpha$ is the accommodation coefficient.[29] The accommodation coefficient is the fraction of the impinging gas molecules that transfer all their momentum to the particle surface before they leave the surface at the interface gas/particle.[28] Based on a published value for $\alpha$ of 0.91 for air, the computed value of $\delta$ is 0.905.[28]

For particles substantially smaller than the mean free path of gas ($d_p << \lambda$; $\lambda = 66$ nm for air at standard temperature and pressure, STP), the active surface can be computed as:[25,30]

$$A_{geometric} = A_{active} = \pi d_p^2 = \text{for } d_p << \lambda \quad \textbf{(4)}$$

The constant in Eq. 1 may be estimated as the product of B (Eq. 2) and $A_{active}$ (Eq. 5):

$$\text{const} = \frac{\lambda}{\delta \alpha} \quad \textbf{(5)}$$

For all particle sizes, including particles larger than the mean free path of air that interact with the fluid as a continuum,

mobility may be computed as:

$$B = \frac{C}{3\pi\eta d_p} \quad (6)$$

where C is the Cunningham slip correction.[30] Equation 1 may be rearranged to estimate the active surface area for these larger particles ($A_{active}$) using mobility Eq. 6:

$$A_{active} = \frac{3\pi\lambda d_P}{C\delta} \quad (7)$$

Thus, the active surface area for larger particles is proportional to particle diameter, not geometric surface area, with C approaching one as particle diameter increases in the region ($d_p >> \lambda$).

Finally, one can estimate the dimensionless ratio of active to geometric surface area ($s_p$) as:

$$s_p = \frac{3\lambda}{C\delta d_p} \quad (8)$$

In Figure 1 a plot of this ratio by particle size shows that the active surface area of a particle transitions from being a good estimate of geometric surface area to a poor one as particle size becomes progressively larger. The term $s_p$ is near one (i.e., active is equivalent to geometric surface area) for the molecular regime where particles are smaller than 0.08 $\mu$m. For particles larger than 0.08 $\mu$m, active surface area becomes progressively smaller than the geometric surface area (i.e., $s_p$ becomes progressively less with increasing particle diameter).

Keller et al.[25] showed that Eq. 1 applies up to 0.75 $\mu$m of particle size by using published mobility and mass coefficient data, regardless of particle shapes (agglomerates or spherical particles), and Ku and Maynard[31] reconfirmed the validity of Eq. 1 below 0.1 $\mu$m using silver agglomerates and spherical particles. They compared the active surface area concentration of monodisperse particle agglomerates measured with two commercially available diffusion charger monitors (model LQ1 DC and model DC 2000 CE; EcoChem Analytics, League City, Texas) with the geometric surface area concentration of the particles derived from scanning mobility particle sizer (SMPS) measurements and the projected particle area concentration from transmission electron microscope analysis. The uncertainty in the experimental values of the geometric physical surface area was estimated to be 20%.[31] They found that diffusion charger measurement of active surface area agreed, with a nominal geometric surface area as well as with surface area estimated from particle mobility diameter, regardless of particle morphology for particles smaller than 100 nm, and accounted for 80% and 63% of the geometric surface area for 150-nm and 200-nm particles, respectively. Further experimental data are needed for larger particle sizes.

## METHODS AND MATERIALS

### Site Descriptions

This study was conducted at an engine machining and assembly facility and an adjacent foundry in Indianapolis, Indiana.[1,2,32] The engine machining and assembly center has over 100,000 $m^2$ of floor space and produced about 1000 6-L diesel engines per day when this work was conducted. This facility was divided into three distinct operational areas with different particulate contaminants:

1. *Block-head-rod (BHR) area*. Engine blocks, cylinder heads, and piston connecting rods were machined in

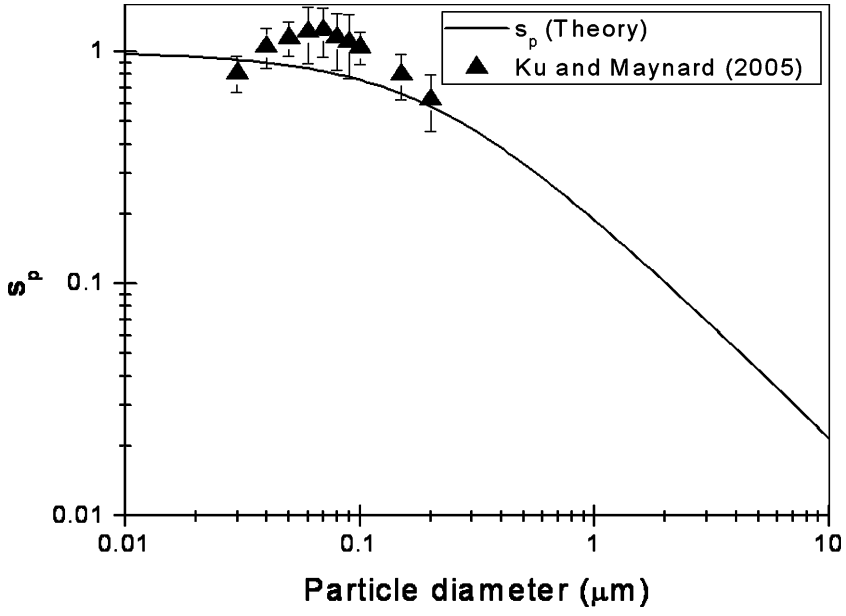


**FIGURE 1.** Fraction of geometric surface area of sphere that is active. This is based on Eq. 8.

transfer lines with state-of-the-art, near-complete ventilation enclosures that used a water-based, synthetic metalworking fluid (MWF). Generally, these ventilated enclosures controlled the aerosol generated by machining operations. Ventilation was provided by 17 air handling units, each processing 23.3 $m^3$/sec (50,000 $ft^3$/min). These units had computer-controlled dampers intended to control the amount of make-up air (outdoor air) and return air (recycled air) in the plant. Air was tempered (heated) in winter with direct-fire natural gas burners or cooled in summer by water-cooled heat exchangers, both within the air handling units. As reported elsewhere, these gas burners were a primary source of ultrafine aerosol that was effectively dispersed throughout this area.[1,32]

2. *Cam-crank (CC) area*. Cam- and crankshafts were machined in transfer lines with older than 20-year-old, loosely fitting enclosures that were retrofitted from previous operations. These machining operations were an obvious source of MWF mist. In this area of the plant, a straight, petroleum-based oil was used as an MWF. In many locations, mist was visible in the air and had formed puddles on the floor. In winter, this area was heated with forced air over steamheated heat exchangers.
3. *Assembly area*. Engines were assembled from a multitude of components. This area of the plant was relatively clean and did not posses obvious sources of aerosol generation.

The 50,000-$m^2$ foundry produced engine blocks and cylinder heads that were used by the adjacent engine facility and at other sites. The foundry was divided into three distinct operational areas:

1. *Core and mold area*. Sand was injected and mechanically pressed to form molds that defined the external surfaces and cores that defined internal voids of the casting. Core and mold components were coated on appropriate surfaces with a water-based binding agent, an emulsion of bentonite, seacoal, soda ash, and a minor constituent of cellulose, and then oven dried. The binding agent served to prevent a burn-in of the sand by the molten alloy during pouring. Core and mold components were assembled and transported to the pour operations by conveyors. These operations mechanically generated dust, but for the most part, emissions appeared to be controlled effectively by local exhaust ventilation.
2. *Melt and pour area*. Iron ingots, scrap metal, and additives were charged into any of eight induction furnaces and melted to produce gray iron alloy. The molten iron alloy was decanted from the furnace into vessels mounted on overhead cranes that transported the molten material to pour areas. Alloy was subsequently poured into mold assemblies for engine blocks and cylinder heads. Fugitive emissions were observed to rise toward large exhaust vents in the roof. Although local exhaust ventilation was in place to capture most of these emissions, some emissions escaped and rose due to thermal convection. Aerosols were generated in this area from metal fume and from partial combustion of combustible material in scrap metal, additives, and hot core and mold components.
3. *Shakeout and cleaning area*. Once solidified and cooled, mold and core material was removed, and the assembly was moved through a lengthy conveyor system, violently shaken by hydraulic rams. The shakeout process separated the majority of the remaining mold and core material from the solidified casting. Castings were further cleaned by an automated shot-blasting process and coarse, dry grinding to remove unwanted material. Components were visually inspected and underwent further manual grinding as needed. Aerosol generation in this area of the facility appeared to be primarily by mechanical means. Most aerosol generated by grinding operations appeared to be effectively controlled by enclosures and ventilation.

## Particle Concentration Mapping

Particle concentrations were mapped throughout both plants as previously described.[1,2,32] Briefly, a condensation particle counter (CPC, model 3007; TSI Inc., Shoreview, Minn.) was used to measure the number concentration of particles with diameters from 10 nm to 1 $\mu$m. An optical particle counter (OPC, PDM-1108; Grimm, Ainring, Germany) was used to measure particle number concentration in 15 channels from 0.3 $\mu$m to 20 $\mu$m. A diffusion charger (DC2000; EcoChem Analytics) was used to measure active surface area concentration ($C_s$). The upper limit for OPC channel 12 is 10 $\mu$m. Data from the OPC were used to calculate respirable aerosol mass concentrations, $C_r$:

$$C_r = \sum_{i=1}^{12} \frac{\pi}{6} \rho_p f_i d_i C_{n,i} \quad \textbf{(9)}$$

where

$f_i$ = fraction of respirable aerosol in channel i computed per ACGIH® criteria[33]
$d_i$ = average of upper and lower boundaries for channel i
$C_{n,i}$ = particle number concentration in channel i (particles/$m^3$) and
$\rho_p$ = assumed unit density of 1 g/$cm^3$

Because the density of the aerosol likely varied with sampling location, a density of 1 g/$cm^3$ was arbitrarily assigned. As described earlier, the respirable mass concentration estimated using Eq. 9 was correlated with gravimetric measurements and underestimated gravimetrically measured concentrations by a factor of approximately 2.[1,2] As discussed in a later section, the relationship among the concentration measurements were analyzed separately for the two different plants, since aerosol properties varied with differing composition resulting from widely varied sources.

Particle number concentrations measured by the CPC were not included in the estimation of mass concentration. The CPC counts particles in the size range of 0.01 to 1 $\mu$m and the

size of the particles measured by the CPC were not measured routinely during the concentration mappings. However, as subsequently demonstrated by ELPI particle number by size measurements, the size of aerosol particles smaller than 0.1 $\mu$m substantially changed with the operation of direct-fire natural gas heaters. In prior studies, less than 20% of the aerosol's mass distribution was attributed to particles smaller than 0.3 $\mu$m.[34] Thus, particles smaller than 0.3 $\mu$m were implicitly assumed to have a negligible effect on respirable aerosol mass. In addition, assessing the sub 0.3 $\mu$m contribution is a practical limitation when relying on optical methods, such as the OPC, to estimate respirable mass concentrations.

This data set consisted of 942 collocated measurements of particle number, active surface area, and respirable mass concentrations. The number of these collocated measurements during spring, summer and winter were 99, 468, and 375, respectively. The fraction of the diffusion charger, active surface area concentration explained by data from the OPC ($F_{a,>0.3\_\mu m}$) was estimated as:

$$F_{a,>0.3\_\mu m} = \frac{\sum_{i=1}^{15} s_{pi} \pi d_i^2 C_{n,i}}{C_s} \quad \textbf{(10)}$$

This term explains the portion of active surface area attributed to particles larger than 0.3 $\mu$m, the smallest particle size detected by the OPC. This term was computed to evaluate the extent to which active surface area concentration is influenced by ultrafine particles.

The number concentration of ultrafine particles ($C_{un}$), with units of particles/cm$^3$, was computed as follows:

$$C_{un} = N_{cpc} - \sum_{i=1}^{5} C_{n,i} \quad \textbf{(11)}$$

where $N_{CPC}$ = particle number concentration measured with the CPC after correction for dilution. The upper boundary of the 5th channel from the OPC was 1 $\mu$m. Thus, $C_{un}$ is the number concentration of particles in the range 0.01 to 0.3 $\mu$m, and it has units of particles/cm$^3$.

## Source Size Distribution Measurements

In summer, aerosol size distributions of selected sources were measured with an electrical low-pressure impactor (ELPI; Dekati Ltd., Tampere, Finland) and the OPC (PDM-1108, Grimm). In the ELPI, a real-time cascade impactor, particles first passed through a diffusion charger, were positively charged, and then collected onto electrically isolated stages by aerodynamic diameter. The current on each stage, measured by electrometers, was further converted into a particle number concentration.[35] ELPI size distributions were obtained every second in 12 channels from 7 nm to 10 $\mu$m. Oiled sintered-metal impaction substrates were used to reduced particle bounce and re-entrainment. The number size distributions measured with the ELPI and OPC were averaged over a period of at least 5 min. Mass weighted size distributions were preferentially derived from the OPC as the upper particle size limit of 20 $\mu$m offered further information. In addition, although number size distributions provided by the ELPI have consistently shown reliability, there remains debate over the validity of mass size distributions derived from the ELPI, with the generation of artifacts on the uppermost stages.[36–39] Consequently, the ELPI data were not used to estimate mass distributions or active surface area distributions as a function of particle size.

## Supply Air Sampling

In summer, sampling equipment was placed downstream of the chiller inside one of the air-handling units that served the BHR area. The system was configured for 100% recirculation of plant air; however, visual inspection indicated that some outside air might have entered the system due to improper functioning of dampers. For the purposes of the present study, the burners were cycled on and off for short durations (5–10 min at 7% of their capacity) with the chiller on. The ELPI was also used to measure aerosol number distributions upstream of the chiller.

## Statistical Analyses

Collocated measurements were analyzed to determine the extent to which ultrafine particle number concentration and respirable mass concentration were predictive of active surface area concentration measured with the diffusion charger. For data collected in winter and summer, this data analysis was conducted on the logarithms of the data. The SAS General Linear Models procedure was used to model the natural logarithm of the active surface area concentration as function of the natural logarithm of the fine particle concentration and as a function of the natural logarithm of the respirable mass concentration. From these analyses, the regression coefficients and the value of $R^2$, the fraction of the variability in the dependent variable that is explained by the independent variable were obtained. The regression model is:

$$\ln(C_s) = (a) + b \ln(X) \quad \textbf{(12)}$$

where

$C_s$ = Active surface area concentration measured by the diffusion charger ($\mu$m$^2$/cm$^3$)
a,b = regression coefficients, and
X = the independent variable, either $C_{un}$ or $C_r$.

In addition, an analysis of covariance was performed on all of the data collected during summer, winter, and spring. The analysis was performed using the SAS General Linear Models procedure. The model for this analysis included: $\ln(C_{un})$ or $\ln(C_r)$; season (spring, summer, or winter); plant (foundry or engine plant); and all interactions involving these variables. This analysis evaluates the extent to which the regression coefficients in equation 12 vary with the season and the plant.

Analyses assume that the residuals (the difference between the modeled and observed values of $\ln(C_s)$ from the analysis) are normally distributed. Much data analysis in the practice of industrial hygiene involves log-normally distributed data.[40] To evaluate this assumption, the Shapiro-Wilk test statistic was computed for the studentized residuals (residual divided by

root mean square error) from the analysis of variance. The SAS Proc Univariate Procedure was used to compute this statistic. In addition, the observed and expected, assuming a log-normal distribution frequency, were plotted. Because the statistical tests revealed that there were statistically significant deviations from normality, the Spearman rank order coefficient was computed using the SAS Proc Corr procedure. Spearman rank-order correlation (r) is a correlation coefficient computed from the ranks of the data values.[41] The range of r is from –1 to 1.

Values of $F_a$ were computed for each mapping location. These data were analyzed to evaluate whether they were affected by season and area within the plant. Each mapping exercise resulted in multiple ratios within each area. All statistical procedures were conducted on the mean of the log-transformed ratio within an area for each mapping session to avoid issues of spatial and temporal correlation. Analysis of variance (Proc GLM SAS) was used to evaluate whether the categorical variables such as season (winter, spring, or summer); area (BHR, CC, or assembly in the engine plant, and core making, melting and pouring, and cleaning areas in the foundry); and their interaction affected $F_a$. To evaluate whether the data were log-normally distributed, the Shapiro-Wilk test statistic was computed for the studentized residuals (residual divided by root mean square error) from the analysis of variance. The SAS Proc Univariate Procedure was used to compute this statistic.

Because the resulting data set did not have an equal number of replicates for each combination of area and season, the least

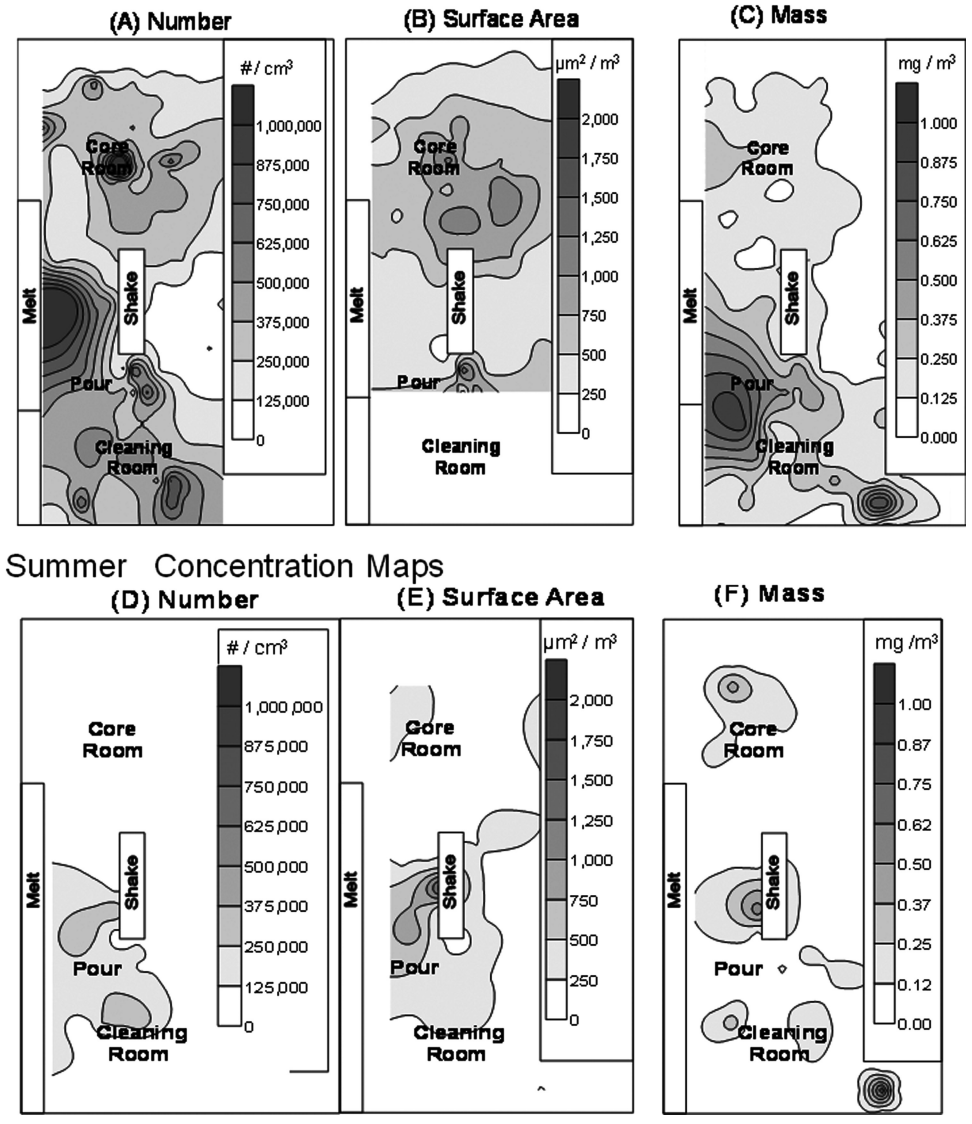


**FIGURE 2.** Map of number, surface area, and mass in foundry in winter and summer.

squares means option of PROC GLM was used to examine differences in these geometric mean values of $F_a$ among the seasons and the difference between seasons at each location. The variance estimate obtained from Proc GLM was used to conduct t-tests to evaluate differences between means. As the resulting data set had between 1 and 4 values for the combinations of season and area, the least squares means (LSM) option was used instead of the multiple comparison tests to examine differences between seasons and the difference between seasons at different locations.

The least square means computation gave equal weight to the different locations and t-tests conducted to examine differences between these geometric means were based upon the root mean square error from the analysis of variance. The geometric means were computed using the LSM option, and t-tests were conducted to evaluate the difference between seasons at these locations. Further statistical analysis was not conducted because the LSM option does not control overall experimental error. Thus, caution is needed interpreting the results of the analysis.

## RESULTS AND FINDINGS

Figure 2 presents example maps of ultrafine number, active surface area, and respirable mass concentrations in the foundry taken from one day in winter and one day in summer. These maps were constructed from data collected simultaneously with different instruments on the same mobile sampling cart. Because of the batch nature of work in the foundry, the aerosol contaminant concentration fluctuated from day to day in the foundry as described by Evans et al.[2] More steady-state conditions were encountered in the engine plant and these concentration maps are available elsewhere.[1] The maps in Figure 2 are provided here to illustrate that different

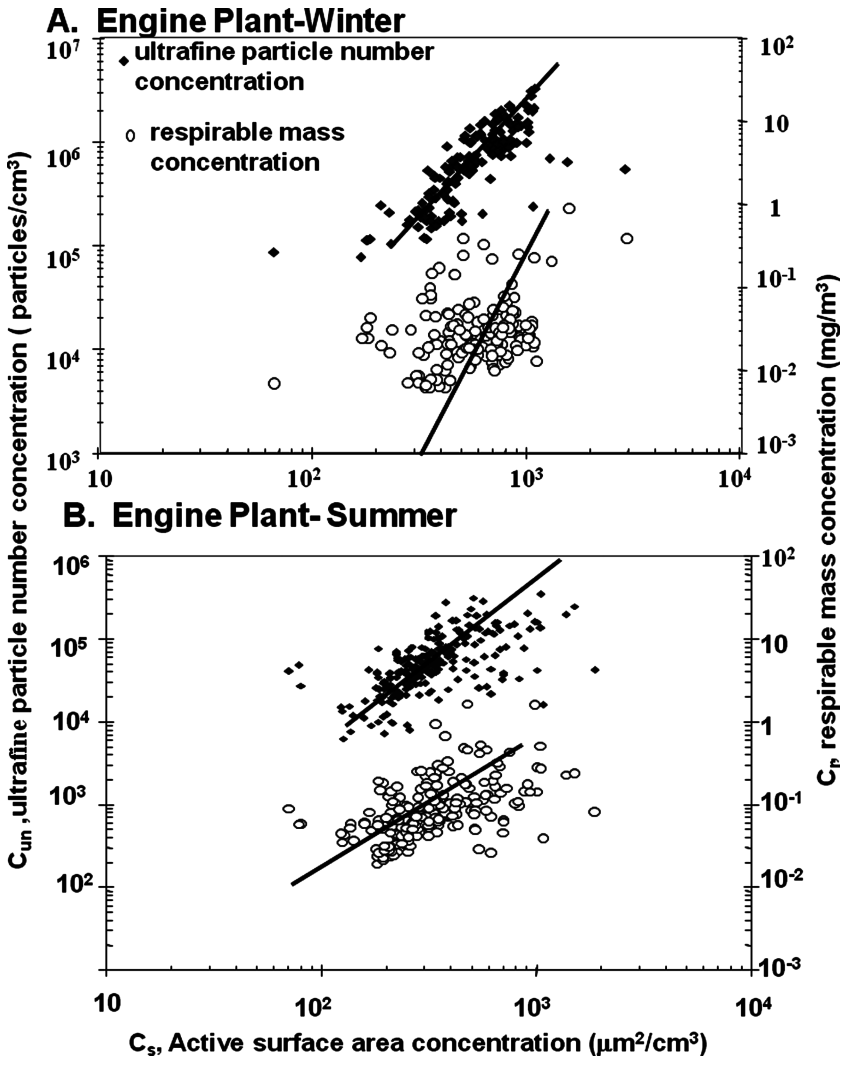


**FIGURE 3.** Relationship between active surface area, particle number, and respirable mass concentrations in the engine plant.

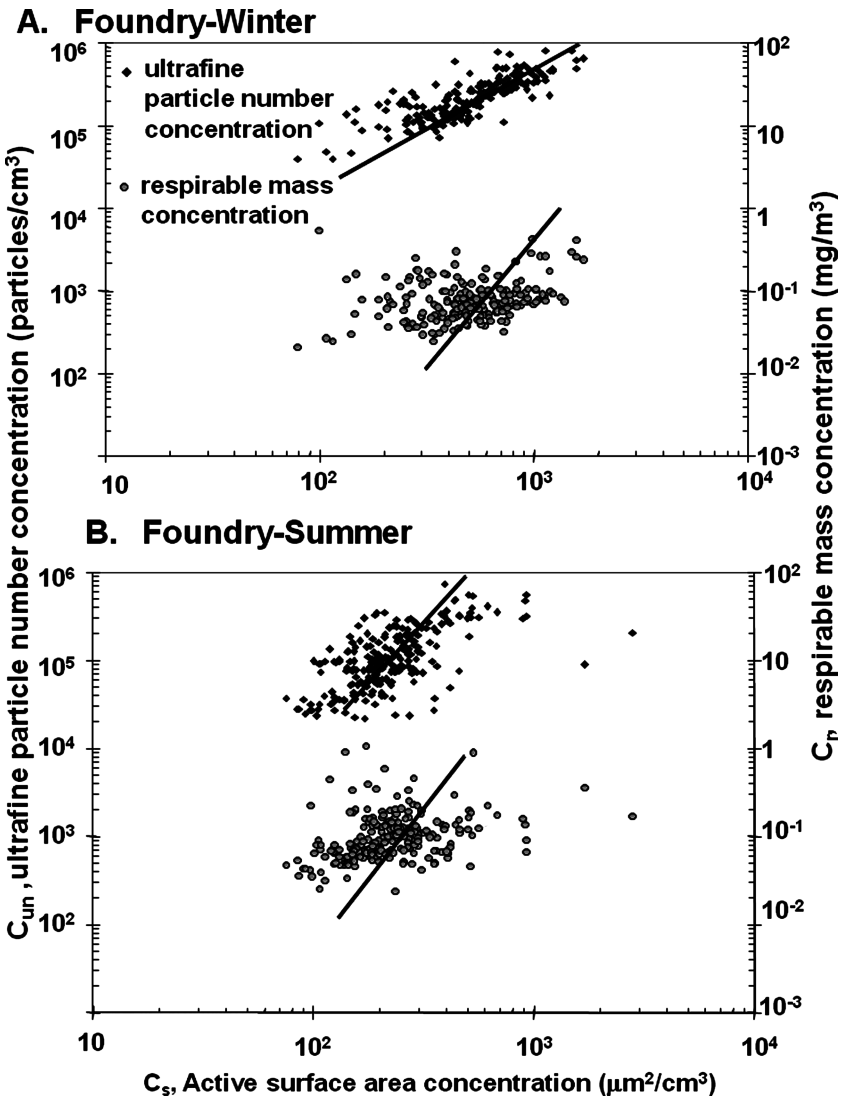


**FIGURE 4.** Relationship between active surface area, particle number, and respirable mass concentrations in the foundry.

metrics provide a substantially different picture of contaminants in the foundry. The greatest number concentrations of ultrafine particles were observed in the melt area, whereas the greatest active surface area concentrations were observed in the core room. The greatest respirable mass concentrations were observed in the cleaning and pouring areas.

Figures 3 and 4 plot ultrafine number and respirable mass concentration as a function of active surface area concentration measured with the diffusion charger. Table I contains the regression statistics for Figures 3 and 4 and the nonparametric Spearman correlation coefficient. Active surface area concentration was more strongly correlated with ultrafine particle number concentration in winter ($R^2 = 0.64$ for engine plant; $R^2 = 0.63$ for foundry; and $r = 0.82$ for both plants) than in summer ($R^2 = 0.37$ and $r = 0.66$ for engine plant; $R^2 = 0.38$ and $r = 0.61$ for foundry). In contrast, active surface area concentration was weakly correlated with respirable aerosol mass concentration in winter ($R^2 = 0.09$ for the foundry; $R^2 = 0.11$ for the engine plant; and $r = 0.29$ for both plants) and in summer ($R^2 = 0.28$ and $r = 0.6$ for the engine plant; and $R^2 = 0.1$ and $r = 0.38$ for the foundry).

The analysis of covariance showed that season significantly ($p = 0.0001$) affected the relationship between the active surface area concentration and the independent variables $\ln(C_{un})$ and $\ln(C_r)$ (Table II). In addition, the relationship between active surface area concentration and ultrafine number concentrations was significantly affected by interaction terms involving season ($p < 0.01$). Plant significantly affected the relationship between active surface area concentration and respirable mass concentration $p = 0.01$).

The regression analysis results presented in Figures 3 and 4 and in Table I assume that the residuals are normally distributed. The tests for normality revealed statistically significant deviations from normality ($p < 0.0001$) for all of the regression analyses. Figure 5 compares the observed distribution of studentized residuals from the analysis of

**TABLE I. Statistics Describing the Relationship Among $C_S$ and the Independent Variables $C_{un}$ and $C_r$**

| | Engine Plant | | | | Foundry | | | |
|---|---|---|---|---|---|---|---|---|
| | Winter | | Summer | | Winter | | Summer | |
| **Figure** | **3A** | **3A** | **3B** | **3B** | **4A** | **4A** | **4B** | **4B** |
| **Independent Variable** | **$C_{un}$** | **$C_r$** | **$C_{un}$** | **$C_r$** | **$C_{un}$** | **$C_r$** | **$C_{un}$** | **$C_r$** |
| Regression Statistics | | | | | | | | |
| Standard Error | 0.29 | 0.45 | 0.41 | 0.44 | 0.33 | 0.52 | 0.39 | 0.47 |
| $R^2$ for regression line, the fraction of the variability explained by the regression model | 0.64 | 0.11 | 0.37 | 0.28 | 0.63 | 0.09 | 0.38 | 0.10 |
| Prob> F from regression analysis | <.0001 | 0.0001 | <.0001 | <.0001 | <.0001 | <.0001 | <.0001 | <.0001 |
| intercept | 0.53 | 6.96 | 1.44 | 6.64 | −2.43 | 6.93 | 0.75 | 6.02 |
| Standard error for intercept | 0.35 | 0.14 | 0.38 | 0.09 | 0.45 | 0.17 | 0.39 | 0.12 |
| Slope | 0.44 | 0.18 | 0.40 | 0.34 | 0.70 | 0.29 | 0.40 | 0.26 |
| Standard error for slope | 0.03 | 0.04 | 0.03 | 0.04 | 0.04 | 0.06 | 0.03 | 0.05 |
| n number | 160 | 160 | 234 | 234 | 215 | 216 | 234 | 234 |
| Nonparametric Statistics | | | | | | | | |
| Spearman correlation coefficient (r) | 0.82 | 0.29 | 0.66 | 0.60 | 0.82 | 0.29 | 0.61 | 0.38 |
| Probability > r | 0.0001 | 0.0002 | 0.0001 | 0.0001 | 0.0001 | 0.0001 | 0.0001 | 0.0001 |

*Note:* The linear regression was performed after taking the natural logarithms of the data.

covariance with a normal distribution. The observed distributions appear to have more of a central tendency than the normal distribution. However, the observed distributions were symmetrically distributed about zero and the distribution of studentized residuals were not visibly skewed. Thus, the distribution of studentized residuals appears to approximate a normal distribution. Furthermore, the interpretation of $R^2$ and r lead to the same interpretation of the data.

**TABLE II. Probability that Independent Variables Affected Active Surface Area Concentration for Models Including the Ultrafine Particle Concentration and the Respirable Mass Concentration**

| | p-Value $C_{un}$ | p-Value $C_r$ |
|---|---|---|
| X ( which is either $\ln(C_{un})$ or $\ln(C_r)$ in Eq. 13) | < 0.0001 | 0.0001 |
| Season | <0.0001 | 0.0001 |
| Plant | p > 0.05 | 0.01 |
| Plant-season interaction | 0.02 | p > 0.05 |
| X-season interaction | <.0001 | p > 0.05 |
| X-plant interaction | p > 0.05 | p > 0.05 |
| X-plant-season interaction | 0.0008 | p > 0.05 |
| Regression Statistics | | |
| $R^2$ | 0.61 | 0.41 |
| Std error of estimate | 0.38 | 0.47 |
| Number of samples | 942 | 942 |

Table III shows the fraction of the active surface area concentration explained by particles larger than 0.3 $\mu$m ($F_{a,>0.3-\mu m}$) by area and season. The values of $F_{a,>0.3-\mu m}$ ranged from 0.08 (block-head-rod area; engine plant; winter) to 0.87 (core area; foundry; summer). This fraction was significantly affected by area of the plant ($p < 0.0001$), season ($p < 0.0001$), and the interaction between season and area ($p < 0.0001$). Values were substantially greater in the summer than in the winter. The residuals from this analysis did not exhibit notable deviations from a log-normal distribution ($p = 0.96$). The LSM estimate of the geometric mean value of $F_{a,>0.3-um}$ during winter, spring, and summer were, respectively, 0.15, 0.36, and 0.62. These means all differed from each other based on t-statistics ($p < 0.0001$).

Figures 6 through Figure 8 present size distribution measurements made at selected locations in both facilities during summer. Ultrafine particles ($d_p < 0.1$ $\mu$m) dominated number concentration in all cases ( Figures 6A, 7A, and 8A.) The greatest concentrations of ultrafine particles were associated with the following hot processes ( Figure 6A): molten alloy pouring in the foundry ($8 \times 10^6$ particles/cm$^3$) and operation of direct-fire gas heaters in the engine plant ($2 \times 10^6$ particles/cm$^3$). These hot processes generated the smallest particles observed in this work (predominately smaller than 0.023 um; Figure 6A). The greatest active surface area concentrations were also found near these processes (2000 $\mu$m$^2$/cm$^3$ for pouring; and 1331 $\mu$m$^2$/cm$^3$ for direct-fire gas heaters).

Whereas aerosol from pouring operations had noticeable mass modes in the 1–10 $\mu$m range (Figure 6B), those from direct-fire gas heaters had little mass associated with particles

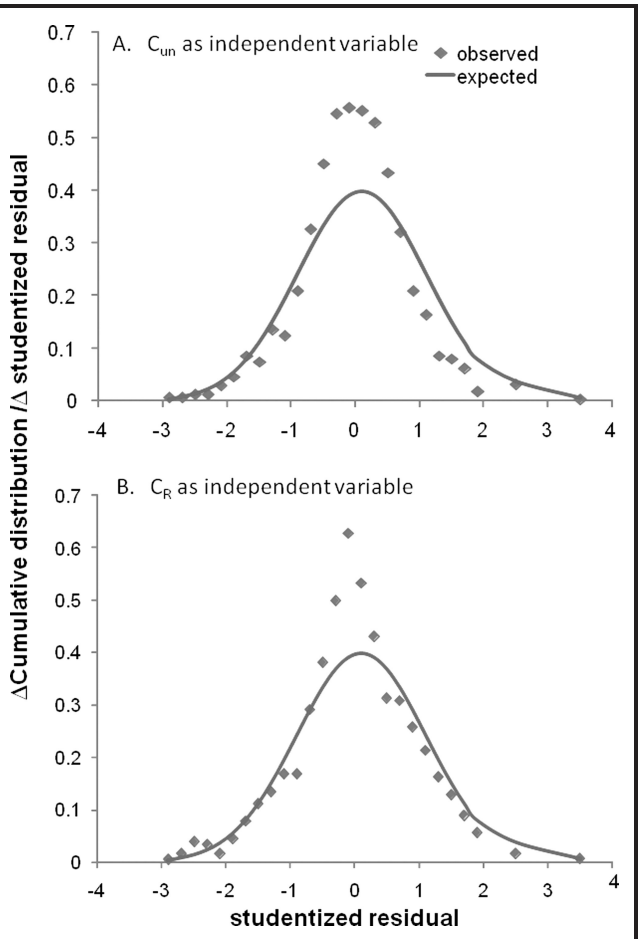


**FIGURE 5.** Frequency distributions of studentized residuals from analysis of covariance. The observed distribution of studentized appears to be approximately consistent with a log-normal distribution.

larger than 1 $\mu$m. Thermal buoyancy caused fugitive emissions from melting and decanting molten alloy to rise to the roof where exhaust fans discharged most emissions out of the foundry. However, the aerosol produced by the operation of the direct-fire gas heaters was directly and deliberately introduced and dispersed into the plants as supply air.

In contrast, other routine foundry and machining operations produced larger aerosol particles ( Figures 7 and 8) than those produced by pouring and direct-fire gas heaters (Figure 6). The ultrafine particle number concentrations and respirable mass concentrations appeared to be influenced differently by particular operations and processes. The mode of the number size distributions for all of these other routine operations were between 0.023 and 0.05 $\mu$m as compared with a mode of less than 0.01 $\mu$m for pouring molten metal and for the direct-fire gas heaters. The aerosol from these other routine operations had substantial mass concentration associated with particles in the 1 $\mu$m to 20 $\mu$m size range. In contrast, the gas-fired heaters produced minimal aerosol mass in this size range (Figure 6B) which was identical to the aerosol in the supply air.

**TABLE III. Fraction of Active Surface Area Concentration Attributed to Particles Detected by the Optical Particle Counter ($F_{a,>0.3\mu m}$)**

| | Winter | | | Summer | | | Prob |
|---|---|---|---|---|---|---|---|
| Area | GM | GSD | n | GM | GSD | n | $> t^A$ |
| Cleaning | 0.35 | | 1 | 0.73 | 1.15 | 3 | 0.007 |
| Core | 0.14 | 1.32 | 3 | 0.87 | 1.20 | 3 | 0.0001 |
| Melt | 0.23 | 1.12 | 3 | 0.49 | 1.26 | 3 | 0.0002 |
| Assembly | 0.09 | 1.15 | 4 | 0.73 | 1.15 | 3 | 0.0001 |
| Block-head-rod | 0.08 | 1.43 | 3 | 0.59 | 1.06 | 3 | 0.0001 |
| Cam-crank | 0.39 | | 1 | 0.78 | 1.16 | 3 | 0.009 |
| Least square means by season[B] | 0.15 | [A] | 18 | 0.62 | [A] | 15 | 0.0001 |

[A]The least square means option in SAS uses the variance estimate from the ANOVA to conduct the t-tests. The geometric standard deviation from this variance estimate was 1.2 with 21 degrees of freedom. Caution is needed interpreting this table as the least squared means tests does not include consideration of overall experimental error. To keep the overall probability of falsely declaring on or more of the difference across seasons significant below 0.01, p in this table needs to be less than 1- $(0.99)^{1/7}$ or 0.0014 as seven differences between winter and summer were evaluated.

[B]Weighted so that all locations have equal influence in the presence of unequal sample sizes.

## DISCUSSION

Areas of greatest concentration in the foundry varied substantially depending on the chosen exposure metric (Figure 2). Ramachandran et al.[42] identified a similar situation for occupational exposure of parking garage attendants to diesel particulate. Thus, the metrics most closely associated with adverse health effects need to be identified so that rational priorities may be set for controlling particulate exposure hazards.

The particle size distribution of an aerosol is integral to the relationship among active surface area, number, and respirable mass concentration. Although active surface area concentration appeared to be a distinct exposure metric, it was more closely related to ultrafine particle number ($R^2$ values ranged from 0.3 and 0.6, r values ranging from 0.6 to 0.8 in Table I) than respirable mass concentration ($R^2$ values ranged from 0.09 to 0.27 and r values ranging from 0.29 to 0.6 in Table I). This observation is explained, at least in part, by the fact that particles progressively larger than 0.1 $\mu$m contribute diminishingly less to active surface area concentration (Figure 1). In this study, active surface area was virtually independent from respirable mass.

The strength of the correlation between the ultrafine particle number and active surface area concentrations depended on season, with the operation of the direct-fire natural gas heaters present in both facilities. The correlation was strongest in winter when particle number size distributions were dominated by ultrafine particles from the heaters. These units introduced

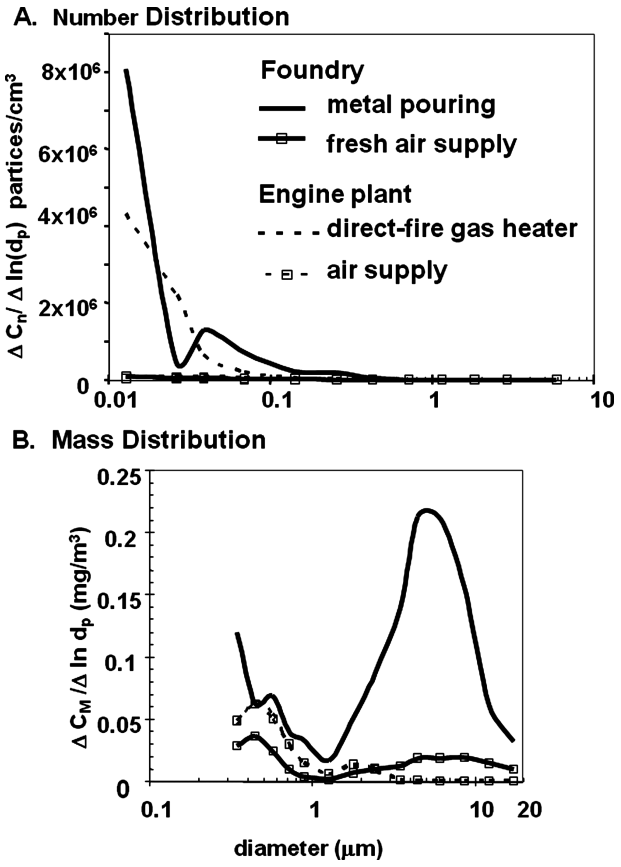


**FIGURE 6.** Number and mass distributions for selected hot processes in both plants. The "metal pouring" and "direct-fire gas heater" produced number concentration distributions that were about a factor of 50 larger than the concentrations in the air supply for the foundry and the engine plant. The metal pouring operation was directly in the plume from pouring metal into a mold. The fresh air sample in the foundry was taken at fresh air supply outlet in the core room. The engine plant samples were taken in the air handling unit with the direct-fire gas heater in use and with this heater off, the sample labeled air supply. The size distributions for the air supply are repeated in Figures 7 and 8.

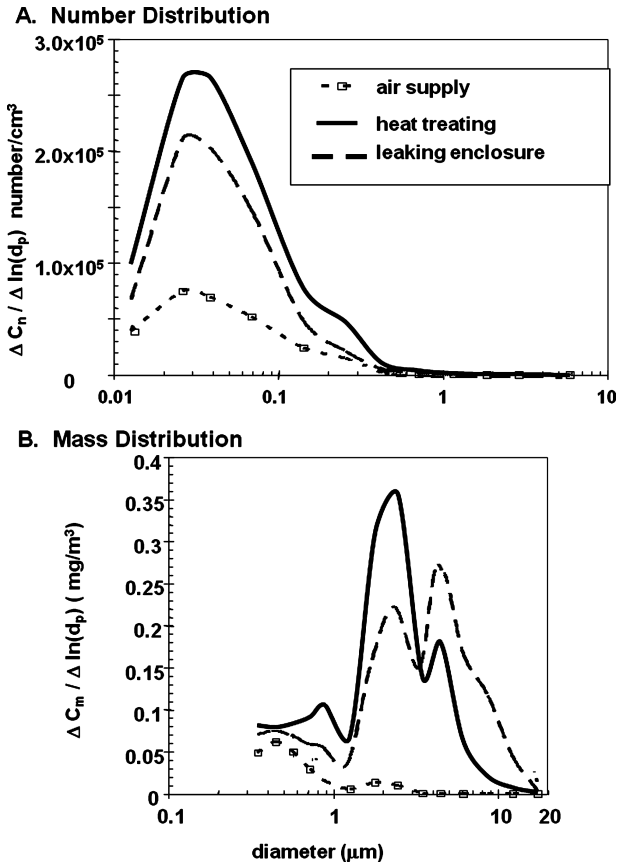


**FIGURE 7.** Selected size distributions in the engine plant. The air supply sample was taken inside the air handling unit while the burners were not in use. The distribution labeled "heat treating" was taken near a heat treating operation in the cam-crank area. The distribution labeled "leaking enclosure" was taken in the block-head-rod area near a tunnel enclosure that was not ventilated adequately.

substantial number concentration ($2 \times 10^6$ particles/cm$^3$) and active surface area concentration (1300 $\mu$m$^2$/cm$^3$) to air supplied throughout both plants. In essence, the correlation during winter was simply the result of diluting and dispersing the particles produced by the heaters.

In summer when the heaters were off, the fraction of the variability in the active surface area explained by the ultrafine particle concentration was substantially less ($R^2$ is 40%) than that in winter ($R^2$ is 60%). In the absence of particle generation by the burners, active surface area exposure was caused by conventional foundry and machining operations. As documented in Table III over all locations in the plant, 62% of the active surface during summer was explained by particles larger than 0.3 $\mu$m as compared with 15% during winter.

From Table III, it is apparent that active surface area concentration may be partially explained by particles larger than 0.3 $\mu$m and active surface area concentration is not exclusively caused by ultrafine particles. This result is problematical in the event that active surface is used as an exposure metric for health effects studies involving nano-materials or ultrafine particles. In the occupational environment, exposures to ultrafines or nanomaterials will occur in combination with exposures to larger aerosols as in metal pouring (see Figure 6). The response of the diffusion charger to particles larger than 0.1 $\mu$m needs to be experimentally determined.

Although this work was limited to two facilities, similar relationships among metrics of exposure are anticipated in other situations because of the physical nature of particle generation, transport, and measurement. As clearly illustrated in Figures 6–8, mechanical processes that generate primarily supermicrometer particles are less potent generators of ultrafine particles than, for instance, hot processes involving combustion or molten alloy. As shown in Figure 6, combustion results in fine and ultrafine particles that dominate particle number and surface area concentrations but often contribute little to particle mass concentrations. Thus, in areas and seasons dominated by combustion aerosol, particle number concentrations should

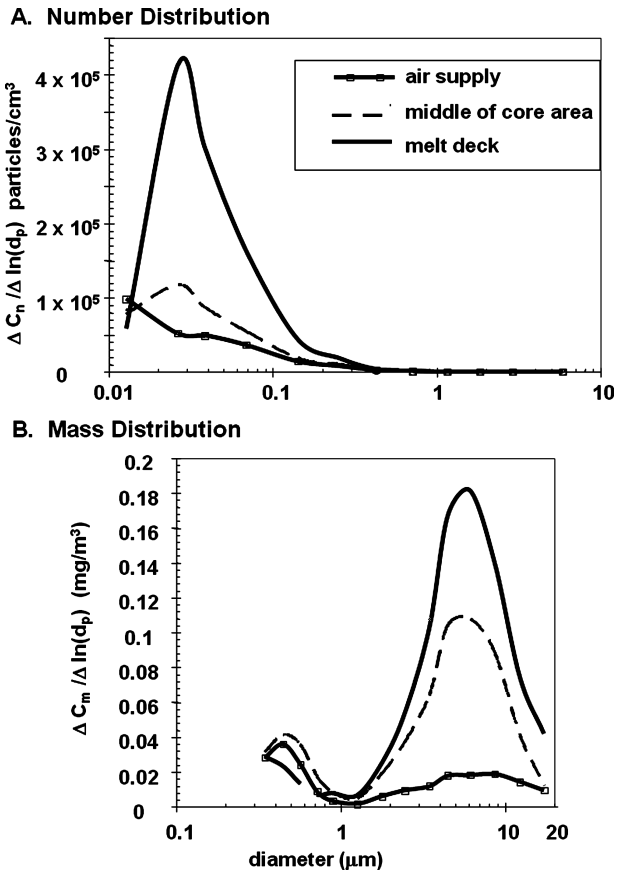


**FIGURE 8.** Selected size distributions in the foundry. The distribution labeled "air supply" was taken at a fresh air supply duct in the middle of the core and mold area. The distribution labeled "middle of core area" was taken away from specific exposure sources in the core and mold area. The distribution labeled "melt deck" was taken on an elevated platform about 5–10 m from furnaces used to melt the iron.

correlate more strongly with active surface area concentrations than in areas dominated by mechanically generated aerosols.

Although considerable uncertainty remains in which exposure metric is most pertinent to protect worker health, multiple metrics are needed to understand exposures to ultrafine particulates or nanomaterials. Number may be closely related to active surface area concentration but both metrics are distinct from mass concentration. Clearly, aerosol size information is needed to understand the relationships between these exposure metrics.

However, in situations where particle sizing in the workplace is impractical, we encourage the use of a condensation particle counter to measure particle number concentration or a diffusion charger to measure active surface area concentration to supplement mass concentration measurements. Both instruments provide a relatively economical means to develop a fuller understanding of particle exposures in the workplace. More frequent use of such instrumentation will help target areas for additional control and provide useful information for epidemiologic studies focused on ultrafine particulate in the workplace.

In addition to measurements in the workplace, simultaneous monitoring of particle number, active surface area, and respirable mass should be conducted during inhalation toxicology studies of fine, ultrafine, or nanostructured materials. As above, these metrics are relatively easy to obtain and the information gained from these studies will be directly comparable to those in the workplace. Thus, appropriate risk assessments and, hence, prudent risk management approaches may be conducted.

## CONCLUSIONS

The active surface area metric is distinct from respirable mass and ultrafine particle number concentration. Particle size distribution dictates how active surface area concentration relates to these metrics. In this study, where sources of ultrafine particles existed, active surface area concentrations were largely explained by particles smaller than 0.1$\mu$m, as in the case of the direct gas-fired heaters. However, in the absence of significant sources of ultrafine aerosol, particles larger than 0.3 $\mu$m accounted for larger fraction of the active surface area concentration.

For a better understanding of the relationships among particle number, surface area, and mass concentrations, workplace particle size distribution measurements are recommended. However, where particle size distribution measurement is impractical, simultaneous measurements of particle number, active surface area and mass concentrations, at a minimum, should be conducted.

## REFERENCES


1. **Heitbrink, W.A., D.E. Evans, T.M. Peters, and T.J. Slavin:** The characterization and mapping of very fine particles in an engine machining and assembly facility. *J. Occup. Environ. Hyg. 4*:341–351 (2007).
2. **Evans, D.E., W.A. Heitbrink, T.J. Slavin, and T.M. Peters:** Ultrafine and respirable particles in an automotive grey iron foundry. *Ann. Occup. Hyg. 52(1)*:9–21 (2008).
3. **Thornburg, J., and D. Leith:** Size distribution of mist generated during metal machining. *Appl. Occup. Environ. Hyg. 15*:618–628 (2000).
4. **Pankow, J.F.:** An absorption model of the gas/particle partitioning of organic compounds in the atmosphere. *Atmos. Environ.* 28(2):185–188 (1994).
5. **Chan, T.L., J.B. D'Arcy, and J. Saik:** Size characteristics of machining fluid aerosols in the an industrial metalworking environment. *Appl. Occup. Environ. Hyg. 5*:162–163 (1990).
6. **Heitbrink, W.A., J.B. D'Arcy, and J.M. Yacher:** Mist generation at a machining center. *Am. Ind. Hyg. Assoc. J.* 61(1):22–30 (2000).
7. **Heitbrink, W.A., J.M. Yacher, G.J. Deye, and A.B. Spencer:** Mist control at machining center, Part 1: Mist characterization. *Am. Ind. Hyg. Assoc. J.* 61(2):275–28 (2000).
8. **Thornburg, J., and D. Leith:** Size distribution of mist generated during metal machining. *Appl. Occup. Environ. Hyg. 15*:618–628 (2000).
9. **Heitbrink, W.A., J.B. D'Arcy, and J.M. Yacher:** Mist generation at a machining center. *Am. Ind. Hyg. Assoc. J. 61(1)*:22–30 (2000).
10. **Lefebvre, A.H.:** *Atomization and Sprays*. New York: Hemisphere Publishing, 1989.

11. **Zimmer, A.T., and P. Biswas:** Characterization of the aerosols resulting from arc welding processes. *J. Aerosol Sci. 32(8)*:993–1008 (2001).
12. **Zimmer, A.T., P.A. Baron, and P. Biswas:** The influence of operating parameters on number-weighted aerosol size distribution generated from a gas metal arc welding process. *J. Aerosol Sci. 33(3)*:519–31 (2002).
13. **Zimmer, A.T, and A.D. Maynard:** Investigation of the aerosols produced by a high-speed hand-held grinder using various substrates. *Ann. Occup. Hyg. 46(8)*:663–672 (2002).
14. **Ross, A.S., K. Teschke, M. Brauer, and S.M. Kennedy:** Determinants of exposure to metalworking fluid aerosol in small machine shops. *Ann. Occup. Hyg. 48(5)*:383–391 (2004).
15. **Portela, J.R., J. Lopez, E. Nebot, and E. Martinez de la Ossa:** Elimination of cutting oil wastes by promoted hydrothermal oxidation. *J. Hazard Mater. 88(1)*:95–106 (2001).
16. **Zarudi, I., and L.C. Zhang:** A revisit to some wheel-workpiece interaction problems in surface. *Int. J. Machine Tools Manufacture 42*:905–913 (2002).
17. **ACGIH:** *2008 TLVs and BEIs Based on the Documentation of the Threshold Limit Values for Chemical Substances and Physical Agents and Biological Exposure Indices*. Cincinnati Ohio, 2008. pp. 1–94.
18. **Brouwer, D.H., J.H.J. Gijsbers, and M.W.M. Lurvink:** Personal exposure to ultrafine particles in the workplace: Exploring sampling techniques and strategies *Ann. Occup. Hyg. 48(5)*:439–453 (2004).
19. **Oberdörster, G., J. Finkelstein, J. Ferin, et al.:** Ultrafine particles as a potential environmental health hazard—Studies with model particles. *Chest 109(Suppl 3)*:68–69 (1996).
20. **Peters, A., H.E. Wichmann, T. Tuch, J. Heinrich, and J. Heyder:** Respiratory effects are associated with the number of ultrafine particles. *Am. J. Respir. Crit. Care Med. 155*:1376–1383 (1997).
21. **Donaldson, K., D. Brown, A. Clouter, et al.:** The pulmonary toxicology of ultrafine particles. *J. Aerosol Med. 15(2)*:213–220 (2002).
22. **Maynard, A.D., and E.D. Kuempel:** Airborne nanostructured particles and occupational health. *J. Nanopart. Res. 7*:587–614 (2005).
23. **Maynard, A.D.:** Estimating aerosol surface area from number and mass concentration measurements. *Ann. Occup. Hyg. 47(2)*:123–144 (2003).
24. **Brunauer, S., P.H. Emmet, and E. Teller:** Adsorption of gases in multimolecular layers. *J. Am. Chem. Soc. 60*:309–319 (1938).
25. **Keller, A., M. Fierz, K. Siegmann, H.C. Siegmann, and A. Filippov:** Surface science with nanosized particles in a carrier gas. *J. Vac. Sci. Technol. 19(1)*:1–8 (2001).
26. **Maynard, A.D.:** Nanotechnology: The next bit thing, or much ado about nothing. *Ann. Occup. Hyg. 51(1)*:1–12 (2007).
27. **Baltensperger, U., E. Weingartener, H. Burscher, and J. Keskinen:** Dynamic mass and surface area measurements. In *Aerosol Measurement Principles, Techniques, and Applications*, 2nd ed. P.A. Baron and K. Willeke (eds.). New York: Wiley InterScience, 2001. pp. 404–405.
28. **Fernandez de la Mora, J., L. de Juan, T. Eichler, and J. Rosell:** Differential mobility analysis of molecular ions and nanometer particles. *Trends Anal. Chem. 17*:328–339 (1998).
29. **Friedlander, S.K.:** *Smoke, Dust, and Haze*. 2nd ed. NewYork: Wiley, 2000. p. 33.
30. **Hinds, W.C.:** *Aerosol Technology—Properties, Behavior, and Measurement of Aerosol Properties*. New York: Wiley-Interscience, 1999. pp. 48–51.
31. **Ku, B.K., and A.D. Maynard:** Comparing aerosol surface-area measurements of monodisperse ultrafine silver agglomerates by mobility analysis, transmission electron microscopy and diffusion charging. *J. Aerosol Sci. 36*:1108–1124 (2005).
32. **Peters, T.M., W.A. Heitbrink, D.E. Evans, T.J. Slavin, and A.D. Maynard:** The mapping of fine and ultrafine particle concentrations in an engine machining and assembly facility. *Ann. Occup. Hyg. 50(3)*:249–257 (2006).
33. **ACGIH:** *2005 TLVs and BEIs Based on the Documentation of the Threshold Limit Values for Chemical Substances and Physical Agents and Biological Exposure Indices*. Cincinnati: Ohio: ACGIH, 2005. p. 75.
34. **Sioutas, C.:** A pilot study to characterize fine particles in the environment of an automotive machining facility. *Appl. Occup. Environ. Hyg. 14*:246–254 (1999).
35. **Marjamäki, M., J. Keskinen, D-R. Chen, and D.Y.H. Pui:** Performance evaluation of the electrical low-pressure impactor (ELPI). *J. Aerosol Sci. 31(2)*:249–261 (2000).
36. **Maricq, M., Xu Ning, and R.E. Chase:** Measuring particle mass emissions the electrical low pressure impactor. *Aerosol Sci. Technol. 40*:68–79 (2006).
37. **Kinsey, J.S., W.A. Mitchell, W.C. Squier, et al.:** Evaluation of methods for the determination of diesel-generated fine particulate matter:Physical characterization results. *J. Aerosol Sci. 37(1)*:63–87 (2006).
38. **Gulijk, V.C., J.C.M. Marijnissen, M. Makkee, J.A. Moulijn, and A. Schmidt-Ott:** Measuring diesel soot with a scanning mobility particle sizer and an electrical low-pressure impactor: Performance assessment with a model for fractal-like agglomerates. *J. Aerosol Sci. 35(5)*:633–655 (2004).
39. **Maricq, M.M., D.H. Podsiadlik, and R.E. Chase:** Size distributions of motor vehicle exhaust PM: A comparison between ELPI and SMPS measurements. *Aerosol Sci. Technol. 33(3)*:239–260 (2005).
40. **Mulhausen, J.R., and J. Damiano:** *A Strategy for Assessing and Managing Occupational Exposures*. Fairfax, Va.: AIHA, 1999.
41. "The Student's SEMSTAT." [Online] Available at http://www.itl.nist.gov/div898/handbook/semstat/semstat-doc.pdf (Accessed May 20, 2008).
42. **Ramachandran, G., D.P. Paulsen, W. Watt, and D. Kittelson:** Mass, surface area and number metrics in diesel occupational exposure assessment. *J. Environ. Monitor. 7*:728–735 (2005).